Journal of Applied Physics

The effect of medium viscosity and particle volume fraction on ultrasound directed self-assembly of spherical microparticles

Cite as: J. Appl. Phys. **131**, 134901 (2022); https://doi.org/10.1063/5.0087303
Submitted: 03 February 2022 • Accepted: 14 March 2022 • Published Online: 01 April 2022

S. Noparast, F. Guevara Vasquez and B. Raeymaekers

AIP Publishing

Journal of Applied Physics ARTICLE scitation.org/journal/jap

The effect of medium viscosity and particle volume fraction on ultrasound directed self-assembly of spherical microparticles

Cite as: J. Appl. Phys. **131**, 134901 (2022); doi: 10.1063/5.0087303
Submitted: 3 February 2022 · Accepted: 14 March 2022 ·
Published Online: 1 April 2022

S. Noparast,[1] F. Guevara Vasquez,[2] and B. Raeymaekers[1,a)]

AFFILIATIONS

[1]Department of Mechanical Engineering, University of Utah, Salt Lake City, Utah 84112, USA
[2]Department of Mathematics, University of Utah, Salt Lake City, Utah 84112, USA

[a)]**Author to whom correspondence should be addressed:** bart.raeymaekers@utah.edu

ABSTRACT

Ultrasound directed self-assembly (DSA) allows organizing particles dispersed in a fluid medium into user-specified patterns, driven by the acoustic radiation force associated with a standing ultrasound wave. Accurate control of the spatial organization of the particles in the fluid medium requires accounting for medium viscosity and particle volume fraction. However, existing theories consider an inviscid medium or only determine the effect of viscosity on the magnitude of the acoustic radiation force rather than the locations where particles assemble, which is crucial information to use ultrasound DSA as a fabrication method. We experimentally measure the deviation between locations where spherical microparticles assemble during ultrasound DSA as a function of medium viscosity and particle volume fraction. Additionally, we simulate the experiments using coupled-phase theory and the time-averaged acoustic radiation potential, and we derive best-fit equations that predict the deviation between locations where particles assemble during ultrasound DSA when using viscous and inviscid theory. We show that the deviation between locations where particles assemble in viscous and inviscid media first increases and then decreases with increasing particle volume fraction and medium viscosity, which we explain by means of the sound propagation velocity of the mixture. This work has implications for using ultrasound DSA to fabricate, e.g., engineered polymer composite materials that derive their function from accurately organizing a pattern of particles embedded in the polymer matrix.

I. INTRODUCTION

Ultrasound directed self-assembly (DSA) allows organizing and orienting particles dispersed in a fluid medium into user-specified patterns, driven by the time-averaged acoustic radiation force that results from scattering of the ultrasound wave.[1] King[2] studied the acoustic radiation force that acts on an incompressible spherical particle dispersed in an inviscid medium, whereas Yosioka and Kawasima[3] extended the theory to include compressibility of the spherical particle. Gorkov[4] summarized earlier work and derived a general acoustic radiation force theory for compressible spherical particles, substantially smaller than the wavelength of the ultrasound wave, dispersed in an inviscid medium. The theory shows that particles subject to a standing ultrasound wave assemble at locations where the acoustic radiation force approaches zero and the acoustic radiation potential is locally minimum, which coincides with the nodes or antinodes of the standing ultrasound wave, depending on the density and compressibility of the particles and the medium.

In contrast with electric[5,6] or magnetic[7,8] external field-based DSA methods, ultrasound DSA is not restricted to electrically conductive or magnetic particles. Additionally, low-attenuation of ultrasound waves in low-viscosity media enables scalability.[9] Based on those advantages, ultrasound DSA finds application in, e.g., non-contact particle manipulation,[10] manipulation of cells in biological experiments[11] and biomedical devices,[12] and filtering of particles in microfluidic devices.[13] Furthermore, integrating ultrasound DSA with freeze casting,[14] mold casting,[15,16] or additive manufacturing[17,18] enables fabricating engineered composite materials with a 3D macroscale geometry and a user-specified pattern of particles embedded in the matrix material. The bulk properties of these engineered materials depend on the properties of the particles and matrix material, the spatial organization of the particles in the

matrix, and the interaction between them.[17] Modifying those parameters changes the properties of the composite material and, thus, accurately tuning the spatial organization of particles in the matrix material allows fabricating engineered composite materials with designer properties. Hence, understanding the relationship between the ultrasound wave field and the patterns in which particles assemble is crucial for using ultrasound DSA as a fabrication method for engineered composite materials with designer properties.

Ultrasound DSA reduces to a "forward problem," which quantifies the patterns of particles that result from a user-specified ultrasound wave field, and an "inverse problem," which determines the ultrasound wave field required to assemble a user-specified pattern of particles. Our research group has previously demonstrated theoretical solutions of the forward and inverse ultrasound DSA problems for spherical particles in two dimensions (2D)[1] and three dimensions (3D)[19] and high aspect ratio particles in 2D[20] and 3D,[21] but only considering inviscid media. Additionally, we have demonstrated experimental validation of the theory in both inviscid[1] and viscous media.[18]

Using ultrasound DSA to fabricate composite materials requires the assembly of particles in a viscous rather than an inviscid medium, such as a thermoset resin or a (photo)polymer resin when integrating ultrasound DSA with, e.g., mold casting[16] and additive manufacturing,[17] respectively. The locations where particles assemble, i.e., the nodes or antinodes of the standing ultrasound wave field, depend on the sound propagation velocity of the mixture of particles and viscous medium, which is a function of the frequency of the ultrasound wave, the compressibility and density of the medium and particles, the medium viscosity, and the particle volume fraction.[22] Thus, accurately assembling user-specified patterns of particles in a viscous medium requires accounting for medium viscosity and particle volume fraction rather than relying on inviscid theory only.

Several approaches exist to calculate these parameters. Phenomenological theory defines the sound propagation velocity based on an effective density and compressibility of the mixture.[23,24] However, this approach is only valid when particles are sufficiently far apart from each other so that interactions between them are negligible, which is not satisfied when, e.g., assembling patterns of closely packed particles and when the sound propagation velocity and density of the particles and medium are similar.[25] Alternatively, multiple-scattering theory predicts the sound propagation velocity based on scattering of an ultrasound wave in a mixture of particles and a viscous medium,[26,27] but it only shows good agreement with experiments for dilute mixtures because it accounts for the acoustic interaction between particles but neglects hydrodynamic interactions that are important in concentrated mixtures.[28] Finally, coupled-phase theory provides an alternative to multiple-scattering theory and considers the hydrodynamic interaction between particles and medium resulting from viscous, inertial, and buoyancy forces.[29] It shows better agreement with experiments than multiple-scattering theory, especially when the sound propagation velocity and density of the particles and medium are dissimilar.[25]

Calculating the acoustic radiation force that acts on spherical particles dispersed in a viscous medium also requires accounting for the medium viscosity.[30] For instance, Settnes and Bruus[31] included viscosity in the acoustic radiation force theory for compressible particles and demonstrated that the acoustic radiation force can deviate by orders of magnitude between the viscous and inviscid theory when a large density contrast exists between the particles and the medium, thus emphasizing the importance of accounting for medium viscosity and particle volume fraction when calculating the acoustic radiation force. However, none of these publications evaluate how the locations where particles assemble change with viscosity, which is critical for using ultrasound DSA as a fabrication method for engineered composite materials with user-specified patterns of particles embedded in the matrix material.

Thus, the objective of this paper is twofold. First, we experimentally measure the locations where particles assemble during ultrasound DSA as a function of medium viscosity and particle volume fraction. Second, we derive an ultrasound DSA theory that accounts for the effect of medium viscosity and particle volume fraction on the location where particles assemble. To solve this problem, we integrate the complex wavenumber from the coupled-phase theory into the Helmholtz equation and we use the boundary element method (BEM) to calculate the ultrasound velocity potential in a 2D solution domain, from which we derive the time-averaged acoustic radiation potential and acoustic radiation force. The particles assemble at the local minima of the time-averaged acoustic radiation potential, where the acoustic radiation force approaches zero. We determine the deviation between locations where particles assemble using viscous and inviscid theory and compare experimental measurements to simulation results, and we clarify the underlying physical phenomena.

II. METHODS AND MATERIALS

A. Experimental demonstration

Figure 1 shows a schematic of the experimental setup, which consists of an acrylic reservoir with two ultrasound transducers (piezoelectric ceramic plate, SM111, center frequency $f_{c,i}$, Steminc,

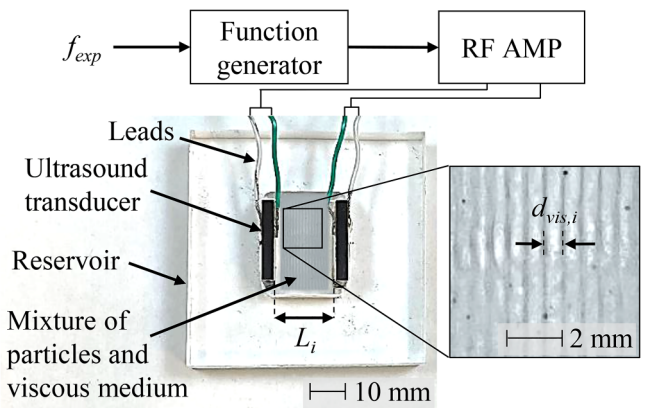

FIG. 1. Schematic of the experimental setup, showing a typical experiment with dimethyl silicone oil 350 cS and borosilicate particles ($\Phi = 0.05$), with $L_2 = 14.40$ mm, $f_{c,2} = 710$ kHz, $N = 20$, and $d_{vis,2} = 0.68$ mm.

FL, USA) affixed to two opposing reservoir walls. The reservoir is filled with a mixture of viscous oil (dimethyl silicone oils 350 and 1000 cS with dynamic viscosity $\eta_{m,1} = 0.34$ and $\eta_{m,2} = 0.97$ Pa s, GT Products, TX, USA) and borosilicate particles (GL0179B/-74 borosilicate glass spheres, average radius $a = 20\,\mu$m, Mo-Sci Corporation, MO, USA). We energize both ultrasound transducers using a function generator (Tektronix AFG 3102) and a radio frequency (RF) power amplifier (E&I 2100L) with the same operating frequency f close to their center frequency $f_{c,i}$ to establish a standing ultrasound wave between both transducers and organize the particles into a pattern of $N = 20$ parallel lines that coincide with the nodes of the standing ultrasound wave. To accomplish this, we use three different reservoirs with lengths $L_1 = 17.33$, $L_2 = 14.40$, and $L_3 = 10.23$ mm, in tandem with ultrasound transducers with $f_{c,1} = 590$ kHz, $f_{c,2} = 710$ kHz, and $f_{c,3} = 1$ MHz, respectively. The inset image of Fig. 1 shows a typical pattern of borosilicate particles (particle volume fraction $\Phi = 0.05$) organized in parallel lines in dimethyl silicone oil 350 cS inside the reservoir with length L_2. The power amplifier supplies 2 and 4 W to the ultrasound transducers for experiments with dimethyl silicone oil 350 and 1000 cS, respectively, which enables driving particles to the nodes of the standing ultrasound wave before they precipitate to the bottom of the reservoir, yet also avoids acoustic streaming, which destroys the patterns of particles.

We experimentally determine the distance between adjacent lines where particles assemble d_{vis} as a function of the medium viscosity η_m and particle volume fraction Φ. However, instead of measuring d_{vis}, which is prone to error, we maintain $d_{vis} = L_i/(N+1)$ constant but measure the operating frequency $f = f_{exp}$ required to establish a standing ultrasound wave that arranges the particles in $N = 20$ parallel lines within the reservoir, for each L_i and corresponding $f_{c,i}$. Specifically, $d_{vis,1} = 0.82$ mm for $L_1 = 17.33$ mm and $f_{c,1} = 590$ kHz; $d_{vis,2} = 0.68$ mm for $L_2 = 14.40$ mm and $f_{c,2} = 710$ kHz; and $d_{vis,3} = 0.49$ mm for $L_3 = 10.23$ mm and $f_{c,3} = 1$ MHz.

Table I shows the material properties of the viscous media and particles we have used in our experiments. Throughout this paper, the subscripts p and m refer to the particle and medium, respectively, when referring to the sound propagation velocity c, density ρ, dynamic viscosity η, and compressibility $\beta = 1/\rho c^2$. We measure the sound propagation velocity in both virgin viscous media c_m (i.e., without particles) using a pulse-echo time-of-flight experiment. We consider a constant sound propagation velocity c_m in each viscous medium, based on the center frequency $f_{c,i}$ of each ultrasound transducer, for all operating frequencies f, because they deviate only slightly from $f_{c,i}$.

We determine f_{exp} for each possible combination of parameters, i.e., a mixture of two viscous media and six different particle volume fractions for three different values of d_{vis} and corresponding L_i and $f_{c,i}$. Prior to each experiment, we disperse the specific particle volume fraction in the viscous medium with sonication (25 W, 2 min, UP200Ht, Hielscher, Teltow, Germany) to minimize particle agglomeration. We initiate each experiment with $f = f_{c,i}$, and we sequentially adjust f in 0.5 kHz intervals until we visually observe the best defined pattern of $N = 20$ parallel lines of particles, when $f = f_{exp}$. For each possible combination of parameters, we perform three repetitions and report the average and minimum and maximum values. We calculate the distance between adjacent lines where particles assemble in an inviscid medium as $d_{inv} = c_m/(2f_{exp})$ and quantify the deviation E_{exp} between adjacent lines where particles assemble in a viscous d_{vis} and an inviscid d_{inv} medium as $E_{exp} = |d_{vis} - d_{inv}|/d_{inv} = |2f_{exp}d_{vis} - c_m|/c_m$. Note that the factor of 2 in d_{inv} accounts for two parallel lines of particles per wavelength.

Furthermore, for each wavelength $\lambda = 2d_{vis}$ and particle volume fraction Φ, we experimentally determine the sound propagation velocity in the mixture of particles and viscous medium $c_{exp} = \lambda f_{exp}$.

B. Theoretical model

We derive a theoretical forward model of ultrasound DSA to predict the locations where particles with radius a (volume fraction Φ) assemble in a viscous medium. Figure 2 displays a schematic of a rectangular reservoir with a mixture of spherical particles and a viscous medium. We use the boundary element method (BEM) to simulate the ultrasound wave field within the reservoir and apply the acoustic radiation force theory for viscous media derived by Settnes and Bruus[31] to calculate the time-averaged acoustic radiation potential U, from which we determine where particles assemble, i.e., at the local minima of U.

Figure 2 shows a simple-closed boundary B with N_b boundary elements that enclose the solution domain D with N_d domain points. The width of the jth boundary element with center point q_j is ε_j. A boundary element represents either a part of the reservoir wall (with velocity $v_j = 0$) or a part of an ultrasound transducer that acts as a piston source with velocity $v_j = v_0 e^{i\omega t - \theta}$ along its normal direction $\boldsymbol{n_j}$, with v_0 being the velocity amplitude and ω and θ being the operating frequency and phase, respectively. We maintain the acoustic impedance Z_b constant along the entire boundary B, whereas the acoustic impedance of the fluid medium is $Z_m = \rho_m c_m$.

We neglect boundary effects confined to the immediate vicinity ($\sim 3\lambda$) of the boundary B and, thus, only simulate the far-field.[9] The time-independent velocity potential φ satisfies the Helmholtz equation throughout the solution domain D, i.e., $\nabla^2\varphi + \tilde{k}^2\varphi = 0$. Here, $\tilde{k}$ is the complex wavenumber that accounts for the effect of the medium viscosity η_m and particle volume fraction Φ on the

TABLE I. Material properties and experimental parameters.

Material	Sound propagation velocity, c (m/s)	Density, ρ (kg/m^3)	Dynamic viscosity, η_m (Pa s)	Radius, a (μm)	Particle volume fraction, Φ
Dimethyl silicone oil, 350 cS	974	970	0.34	…	0–0.250
Dimethyl silicone oil, 1000 cS	983	970	0.97	…	0–0.125
Borosilicate glass spheres	5500	2600	…	20	…

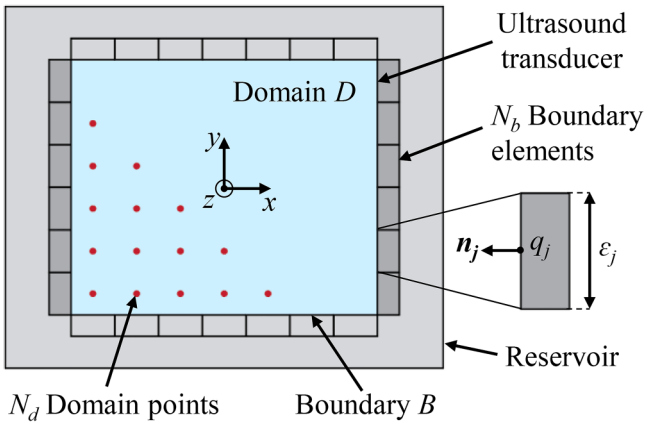

FIG. 2. Rectangular reservoir with a mixture of particles and a viscous medium.

sound propagation velocity (real part) and wave attenuation (imaginary part) of the mixture, given in the coupled-phase theory as[25]

$$\widetilde{k}^2 = \omega^2[(1-\Phi)\beta_m + \Phi\beta_p] \times \frac{\rho_m[\rho_p(1-\Phi+\Phi S)+\rho_m S(1-\Phi)]}{\rho_p(1-\Phi)^2+\rho_m[S+\Phi(1-\Phi)]}, \tag{1}$$

with $\omega = 2\pi f$, f is the operating frequency of the ultrasound wave field, and $S = Q + iR$. $Q = 1/2[(1+2\Phi)/(1-\Phi)] + 9/4(\delta/a)$, $R = 9/4(\delta/a + \delta^2/a^2)$, $\delta = (2\eta_{eff}/\omega\rho_m)^{1/2}$ is the viscous boundary layer thickness around a particle, and $i = (-1)^{1/2}$. We calculate the effective viscosity of the mixture as $\eta_{eff} = (1 + 2.5\Phi + 7.349\Phi^2)$.[25] Additionally, the impedance boundary condition $\partial\varphi/\partial n + i\widetilde{k}\widetilde{Z}\varphi = v$ exists along boundary B, with $\widetilde{Z} = Z_m/Z_b$, which accounts for absorption and reflection of the ultrasound wave at the boundary B. We use the BEM based on Green's theorem to calculate the velocity potential φ in all domain points.[1]

The time-averaged acoustic radiation potential U in a viscous medium is given as[31]

$$U = \frac{4\pi}{3}a^3\left(f_1\frac{\beta_m}{2}\langle p^2\rangle - f_2\frac{3\rho_m}{4}\langle v^2\rangle\right), \tag{2}$$

where the $\langle\bullet\rangle$ operator represents the time-average over one wave period, and the velocity and pressure fields in the solution domain D derive from the velocity potential φ as $v = \nabla\varphi$ and $p = i\rho\omega\varphi$.[31] $f_1 = 1 - \beta_p/\beta_m$ is the monopole scattering coefficient, and $f_2 = \Re\{[2(1-\gamma)(\rho_p/\rho_m - 1)]/[2\rho_p/\rho_m + 1 - 3\gamma]\}$ is the dipole scattering coefficient, with $\gamma = -3/2[1 + i(1+\delta/a)]\delta/a$. $\Re\{\bullet\}$ indicates the real part of the expression. The acoustic radiation force $F = -\nabla U$ drives particles to locations where $F = 0$ and F points toward these locations in their immediate vicinity, which coincides with locations where U is locally minimum.

We simulate a 2D solution domain D that replicates our experiments, including the dimensions of the reservoir L_i, medium viscosity η_m, and particle volume fraction Φ, and we also simulate the methodology of the experiments. For each parameter combination, we determine the operating frequency $f = f_{sim}$ that minimizes the average of the local minima of the time-averaged acoustic radiation potential U in the $N = 20$ locations where particles assemble, by simulating U for each $0.975f_{exp} \le f \le 1.025f_{exp}$, with 0.5 kHz intervals. Here, f_{exp} is the operating frequency for each experiment we perform (d_{vis}, η_m, Φ) that assembles the pattern of $N = 20$ parallel lines of particles. Hence, the simulations match the experimental methodology. Correspondingly, locations where particles assemble are identical in the simulations and experiments because we maintain $N = 20$ and, thus, the distance between adjacent local minima of U is d_{vis}. We calculate the distance between adjacent local minima of U in an inviscid medium as $d_{inv} = c_m/(2f_{sim})$. The simulated deviation of the distance between locations where particles assemble with viscous and inviscid ultrasound DSA theory is $E_{sim} = |d_{vis} - d_{inv}|/d_{inv} = |2f_{sim}d_{vis} - c_m|/c_m$.

Furthermore, for each wavelength $\lambda = 2d_{vis} = 2\pi/\Re\{\tilde{k}\}$ and particle volume fraction Φ, we solve Eq. (1) for ω and determine the sound propagation velocity in the mixture of particles and viscous medium $c_{th} = \lambda\omega/2\pi$.

III. RESULTS AND DISCUSSION

Figures 3(a) and 3(b) show the percent deviation of the distance between adjacent locations where particles assemble in a viscous and inviscid medium as a function of particle volume fraction Φ, and for different values of d_{vis} [$d_{vis,1} = 0.82$ mm (black dot), $d_{vis,2} = 0.68$ mm (blue square), $d_{vis,3} = 0.49$ mm (red triangle), which correspond to different sizes of the reservoir L_i and ultrasound transducers with different $f_{c,i}$. We show both experimental results E_{exp} (solid markers) and simulation results E_{sim} (hollow markers) for medium viscosity $\eta_m = 0.34$ Pa s in Fig. 3(a) and $\eta_m = 0.94$ Pa s in Fig. 3(b). The solid markers show the arithmetic mean of three E_{exp} measurements, and the error bars show the minimum and maximum values, whereas the hollow markers show a single simulation. In Fig. 3(b), we limit the particle volume fraction $\Phi \le 0.125$ for the experimental results (solid markers) for practical reasons; medium viscosity $\eta_m = 0.94$ Pa s in combination with $\Phi > 0.125$ causes high viscosity and attenuation of the ultrasound waves that prevent reliable assembly of particles in parallel lines. We derive third order polynomial best-fit equations of the E_{sim} data points, which predict the deviation between locations where particles assemble when using viscous versus inviscid theory for ultrasound DSA. Conversely, it also allows an ultrasound DSA-user to determine whether to use viscous or inviscid theory to predict the locations where particles will assemble, based on the deviation for specific operating parameters (d_{vis}, η_m, Φ) and the required accuracy.

Additionally, Figs. 3(c) and 3(d) show the sound propagation velocity c in a mixture of spherical particles and viscous medium as a function of the particle volume fraction Φ, for different values of d_{vis} and for medium viscosity $\eta_m = 0.34$ Pa s in Fig. 3(c) and $\eta_m = 0.94$ Pa s in Fig. 3(d). We show experimental results c_{exp} with different markers and the theoretical solution c_{th} from Eq. (1) with different line types.

From Fig. 3, we observe that E first increases and then decreases with increasing particle volume fraction Φ, independent of η_m and

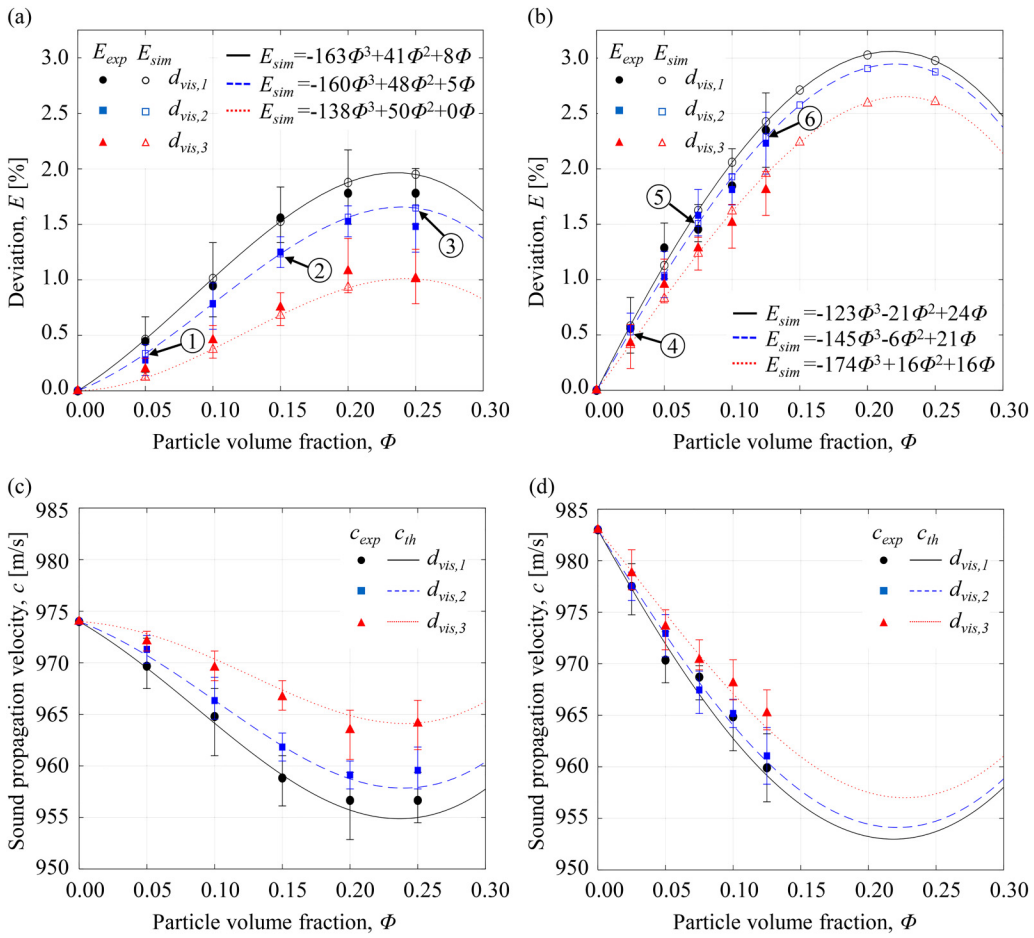

FIG. 3. Percent deviation E_{exp} (solid markers) and E_{sim} (hollow markers) of the distance between adjacent locations where particles assemble in a viscous and inviscid medium as a function of particle volume fraction Φ, for $d_{vis,1} = 0.82$ mm (black dot), $d_{vis,2} = 0.68$ mm (blue square), $d_{vis,3} = 0.49$ mm (red triangle), and for medium viscosity (a) $\eta_m = 0.34$ Pa s and (b) $\eta_m = 0.94$ Pa s. The lines represent best-fit equations of the simulated data (hollow markers). The sound propagation velocity in the mixture of viscous medium and spherical particles based on experiments c_{exp} (markers) and theory c_{th} (lines) as a function of particle volume fraction Φ, for $d_{vis,1}$ (black dot/solid line), $d_{vis,2}$ (blue square/dashed line), $d_{vis,3}$ (red triangle/dotted line), and for medium viscosity (c) $\eta_m = 0.34$ Pa s and (d) $\eta_m = 0.94$ Pa s.

d_{vis}, which results from competing mechanisms. First, the effective viscosity η_{eff} of the mixture increases with increasing Φ, which increases the viscous layer thickness δ around each particle and, thus, increases the drag force it experiences when moving in the viscous medium during ultrasound DSA.[25] Increasing Φ also increases the number of particles in a specific control volume within the mixture. Together, these two phenomena decrease the rate of momentum transfer in the mixture,[25] which decreases the sound propagation velocity of the mixture $c \leq c_m$ and, thus, increases $E = |d_{vis} - d_{inv}|/d_{inv} = |2fd_{vis} - c_m|/c_m = |c - c_m|/c_m$, considering that the distance between adjacent lines of particles $d_{vis} = c/(2f)$. E and f may either have the *exp* or *sim* subscript as it is valid for both the experimental and simulation results. On the other hand, increasing Φ also increases the density and decreases the compressibility of the mixture.[25] For the parameters considered in this work, the ratio of medium to particle compressibility is much larger than the ratio of particle to medium density and, thus, the sound propagation velocity of the mixture $c = (1/\rho\beta)^{0.5} \leq c_m$ increases with increasing Φ, which decreases E. We verify that the particle volume fraction Φ for which E is maximum [see Figs. 3(a) and 3(b)] corresponds to Φ for which the sound propagation velocity of the mixture is minimum [see Figs. 3(c) and 3(d)], independent of $d_{vis,i}$ and η_m.

Furthermore, we observe from Fig. 3 that E increases with increasing d_{vis} and, correspondingly, decreasing operating frequency f. The viscous layer thickness $\delta = (2\eta_{eff}/\omega\rho_m)^{1/2}$ around a particle increases with decreasing operating frequency $f = \omega/2\pi$, which increases the drag force on a particle driven through the mixture by the acoustic radiation force and, in turn, decreases the rate of momentum transfer in the mixture, which decreases the sound propagation velocity $c \leq c_m$ and increases E.

Comparing Figs. 3(a) and 3(b), we observe that E_{sim} increases with increasing η_m (and η_{eff}), which increases the viscous layer

thickness δ around a particle and, thus increases the drag force on particles. Consequently, it decreases the rate of momentum transfer in the mixture, which decreases the sound propagation velocity c and increases E.

We note that the percent deviation between adjacent locations where particles assemble using viscous and inviscid theory is small (<3%). However, it multiplies over the entire scale of the experiment and, thus, increases in importance when using ultrasound DSA to manufacture macroscale material specimens. Additionally, we note that we calculate the percent deviation between locations where particles assemble using viscous and inviscid theory, but we use the viscosity of the dimethyl silicon oil in the inviscid theory. However, when determining the deviation between adjacent locations where particles assemble with viscous theory for a viscous medium and inviscid theory using an inviscid medium such as water at standard temperature and pressure ($\eta = 0.001$ Pa s), we observe the same trends as those depicted in Fig. 3, but the maximum deviation reaches 35%. Evidently, using inviscid theory with an inviscid medium is not a good predictor for locations where particles assemble in a viscous medium because the sound propagation velocity in water ($c_m = 1490$ m/s) is substantially higher than that in the viscous medium (see Table I), which affects the wavelength of the standing ultrasound wave and, thus, the locations of its nodes.

Finally, we mark six numbered labels in Figs. 3(a) and 3(b) to illustrate both the experimental and simulation results of selected individual data points. Figure 4(a) illustrates the experimental results for each numbered label (solid markers in Fig. 3), showing lines of aligned particles (dark) in a viscous medium (bright), whereas Fig. 4(b) shows the corresponding simulation results (hollow markers in Fig. 3) of the time-averaged acoustic radiation potential U, with blue contour lines indicating local minima. Figure 3 shows good quantitative agreement between E_{exp} and E_{sim}, which the images of individual data points in Fig. 4 illustrate. For each numbered label, we observe good agreement between the simulated acoustic radiation potential and the corresponding experimental results that show where particles assemble, including details of the standing ultrasound wave field, which is remarkable. We determine a maximum absolute difference between experiments E_{exp} and simulations E_{sim} of 0.21% (for $d_{vis,1} = 0.82$ mm, $\eta_m = 0.97$ Pa s, $\Phi = 0.10$).

Differences in the experimental and simulation results are likely due to imperfections in fabricating the experimental setup, including the imperfect rectangular shape of the reservoir and the alignment of the ultrasound transducers. Furthermore, the spherical particles are denser than the viscous medium in our experiment, which causes them to sink while subject to the ultrasound wave field. This may create a non-uniform spatial distribution of the particles orthogonal to the wave propagation direction (z direction in Fig. 2) and increases the particle volume fraction at the bottom of the reservoir, thus affecting the sound propagation velocity. We also use a constant average particle radius $a = 20\,\mu$m in our simulations. However, 90% of the particles have radius $a \leq 37\,\mu$m and 50% of particles have radius $18 \leq a \leq 22\,\mu$m. Hence, this may affect the sound propagation velocity of the mixture c. Finally, imperfect dispersion of particles in the viscous medium prior to the start of each experiment may also cause inaccuracy. Increasing particle volume fraction increases particle agglomeration, thus changing the effective particle size, and it also increases ultrasound attenuation, which decreases the acoustic radiation force that acts on the particles in the mixture. Each of these effects potentially distorts and fades the pattern of particles.

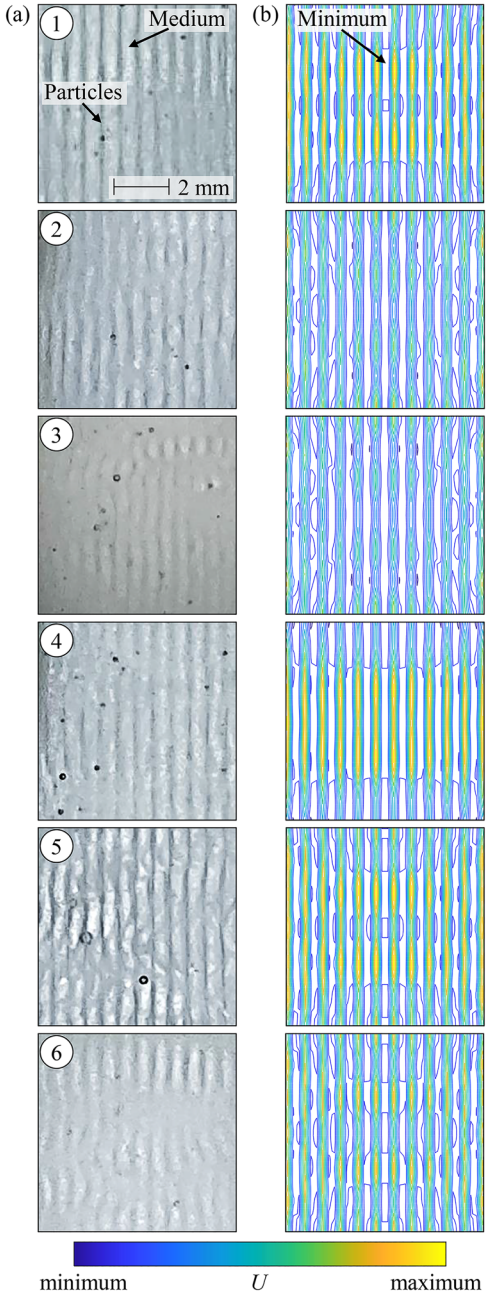

FIG. 4. (a) Experimental results for each numbered label in Fig. 3, showing lines of aligned particles (dark) in viscous medium (bright), and (b) the corresponding simulation results of the time-averaged acoustic radiation potential U.

We also emphasize that the viscous DSA theory we have implemented in our simulations determines the locations where particles assemble in a viscous medium, accounting for both medium viscosity η_m and particle volume fraction Φ, which are different than where they assemble in an inviscid medium. This builds on the theory of Settnes and Bruus,[31] which describes the acoustic radiation force that acts on spherical particles in a viscous medium as a function of medium viscosity but did not determine or discuss the locations where particles assemble.

IV. CONCLUSION

In conclusion, the steady-state locations where spherical particles organize during ultrasound DSA are different in a viscous and inviscid medium and depend on particle volume fraction Φ and medium viscosity η_m. We experimentally measure the deviation between locations where particles assemble as a function of particle volume fraction Φ, medium viscosity η_m, and operating frequency f. In addition, we simulate the experiments by implementing an ultrasound DSA simulation that integrates the Helmholtz equation with a complex wave number $\tilde{k}$ to account for particle volume fraction Φ, in combination with the acoustic radiation potential theory that accounts for medium viscosity η_m. The maximum absolute difference between experiments and simulations is 0.21%. We provide best-fit equations to predict the deviation between locations where particles accumulate during ultrasound DSA in viscous and inviscid media. The deviation increases with increasing particle volume fraction and medium viscosity because the sound propagation velocity of the mixture of particles and viscous medium changes compared to that of the inviscid medium. When considering ultrasound DSA of a periodic pattern of lines of particles, we determine a 3% maximum deviation between adjacent particle locations but note that this deviation scales with the dimensions of the experiment/simulation. These results have implications for using ultrasound DSA as a fabrication process for, e.g., engineered polymer composite materials whose properties depend on the spatial organization of patterns of particles in the matrix material.

ACKNOWLEDGMENTS

This research was supported by the National Science Foundation under Award No. 2017588.

AUTHOR DECLARATIONS

Conflict of Interest

The authors have no conflicts to disclose.

DATA AVAILABILITY

The data that support the findings of this study are available from the corresponding author upon reasonable request.

REFERENCES

[1]J. Greenhall, F. Guevara Vasquez, and B. Raeymaekers, Appl. Phys. Lett. **108**, 103103 (2016).
[2]L. V. King, Proc. R. Soc. A **147**, 212 (1934).
[3]K. Yosioka and Y. Kawasima, Acustica **5**, 167 (1955).
[4]L. P. Gorkov, Sov. Phys. Dokl. **6**, 773 (1962).
[5]Z. Guo, J. A. Wood, K. L. Huszarik, X. Yan, and A. Docoslis, J. Nanosci. Nanotechnol. **7**, 4322 (2007).
[6]Y. Yang, Z. Chen, X. Song, Z. Zhang, J. Zhang, K. K. Shung, Q. Zhou, and Y. Chen, Adv. Mater. **29**, 1605750 (2017).
[7]J. H. E. Promislow and A. P. Gast, Langmuir **12**, 4095 (1996).
[8]J. J. Martin, B. E. Fiore, and R. M. Erb, Nat. Commun. **6**, 8641 (2015).
[9]L. E. Kinsler, A. R. Frey, A. B. Coppens, and J. V. Sanders, *Fundamental of Acoustic*, 4th ed. (John Wiley & Sons, Inc., New York, 2000), p. 210, ISBN: 0471847895, ISBN-13: 9780471847892.
[10]X. Ding, S. C. S. Lin, B. Kiraly, H. Yue, S. Li, I. K. Chiang, J. Shi, S. J. Benkovic, and T. J. Huang, Proc. Natl. Acad. Sci. U.S.A. **109**, 11105 (2012).
[11]M. Evander and J. Nilsson, Lab Chip **12**, 4667 (2012).
[12]Y. Yamakoshi, Y. Koitabashi, N. Nakajima, and T. Miwa, Jpn. J. Appl. Phys. **45**, 4712 (2006).
[13]B. Jung, K. Fisher, K. D. Ness, K. A. Rose, and R. P. Mariella, Anal. Chem. **80**, 8447 (2008).
[14]T. A. Ogden, M. Prisbrey, I. Nelson, B. Raeymaekers, and S. E. Naleway, Mater. Des. **164**, 107561 (2019).
[15]M. D. Haslam and B. Raeymaekers, Compos. Part B **60**, 91 (2014).
[16]J. Greenhall, L. Homel, and B. Raeymaekers, J. Compos. Mater. **53**, 1329 (2019).
[17]K. Niendorf and B. Raeymaekers, Adv. Eng. Mater. **23**, 2001002 (2021).
[18]J. Greenhall and B. Raeymaekers, Adv. Mater. Technol. **2**, 1700122 (2017).
[19]M. Prisbrey, J. Greenhall, F. Guevara Vasquez, and B. Raeymaekers, J. Appl. Phys. **121**, 014302 (2017).
[20]M. Prisbrey and B. Raeymaekers, Phys. Rev. Appl. **12**, 014014 (2019).
[21]M. Prisbrey, F. Guevara Vasquez, and B. Raeymaekers, Appl. Phys. Lett. **117**, 111904 (2020).
[22]J. M. Evans and K. Attenborough, J. Acoust. Soc. Am. **102**, 278 (1997).
[23]R. J. Urick, J. Appl. Phys. **18**, 983 (1947).
[24]W. S. Ament, J. Acoust. Soc. Am. **25**, 638 (1953).
[25]A. H. Harker and J. A. G. Temple, J. Phys. D: Appl. Phys. **21**, 1576 (1988).
[26]P. S. Epstein and R. R. Carhart, J. Acoust. Soc. Am. **25**, 553 (1953).
[27]J. R. Allegra and S. A. Hawley, J. Acoust. Soc. Am. **51**, 1545 (1972).
[28]D. J. McClements, J. Acoust. Soc. Am. **91**, 849 (1992).
[29]W. H. Schwarz, J. Acoust. Soc. Am. **96**, 319 (1994).
[30]A. A. Doinikov, J. Acoust. Soc. Am. **101**, 713 (1997).
[31]M. Settnes and H. Bruus, Phys. Rev. E **85**, 016327 (2012).